ORIGINAL PAPER

Global variable compact multipoint methods for accurate upscaling with full-tensor effects

**Tianhong Chen · Margot G. Gerritsen ·
James V. Lambers · Louis J. Durlofsky**

Abstract New transmissibility upscaling procedures designed to accurately capture full-tensor effects are developed and applied. These techniques are based on variable compact multipoint (VCMP) flux approximations. VCMP is extended to irregular grids. Two approaches for including global flow information within the VCMP upscaling procedure are considered—one in which the upscaled model is determined directly and one in which iteration of the coarse-scale model is used to minimize the mismatch between coarse-scale fluxes and integrated fine-scale fluxes. To guarantee monotonicity, the VCMP stencils are adapted to assure the coefficient matrix is an M-matrix whenever nonmonotone solutions are encountered. The new VCMP procedures are applied to multiple realizations of two-dimensional fine-scale permeability descriptions for coarse models defined on both Cartesian and irregular quadrilateral grids. Both log-normally distributed permeability fields with oriented layers and channelized models are considered. Six different upscaling techniques (extended local, direct global, and iterated global, each using both two-point and VCMP flux approximations) are assessed for four different sets of global boundary conditions. The global VCMP techniques consistently display high degrees of accuracy for total flow rate, L_2 flux error, and L_2 pressure error. For the oriented-layer cases, where full-tensor effects are important, the global VCMP methods are shown to provide clearly better overall accuracy than analogous methods based on two-point flux approximations. For channelized cases in which full-tensor effects are not significant, both types of methods provide high levels of accuracy. The selective M-fix procedure is also shown to lead to improved accuracy, which can be significant in some cases. In total, for the systems considered here, the new global VCMP upscaling techniques are observed to provide the best overall accuracy of any of the upscaling methods investigated.

Keywords Upscaling · Two-point flux approximation (TPFA) · Variable compact multipoint (VCMP) · Transmissibility · Full-tensor permeability · Heterogeneity · Multiscale · Reservoir simulation · Subsurface flow

PACS 47.11.St · 47.56.+r · 47.11.Df · 92.40.Kf · 92.40.-t

T. Chen · M. G. Gerritsen (✉) · J. V. Lambers ·
L. J. Durlofsky
Department of Energy Resources Engineering,
Stanford University, Stanford, CA, 94305-2220, USA
e-mail: margot.gerritsen@stanford.edu

T. Chen
e-mail: thchen@stanford.edu

J. V. Lambers
e-mail: lambers@stanford.edu

L. J. Durlofsky
e-mail: lou@stanford.edu

1 Introduction

A typical geocellular model of a heterogeneous oil reservoir may contain on the order of 10^7 to 10^8 cells. Although feasible, numerical simulations using such large geological models are usually still far too expensive for realistic applications. This is because, in practice, multiple simulations must be performed in order

to choose among various recovery or well placement strategies. In addition, the impact of reservoir uncertainty is typically quantified by simulating a large number of geostatistical realizations of the reservoir [3]. For these reasons, geological models are usually upscaled by a factor of 10 to 1,000 in practical reservoir simulation settings. Our objective in this work is to extend existing upscaling capabilities to provide more accurate coarse-scale models while accommodating general permeability anisotropy and irregular quadrilateral grids.

Within the context of subsurface flow modeling, the most fundamental property considered for upscaling is the rock permeability (designated k). Upscaling of permeability has been an active area of research, and extensive reviews of existing methods are given in [9, 12, 13, 26], among others. Methods can be classified as permeability or transmissibility upscaling procedures depending on the coarse-scale property computed. Permeability upscaling methods entail the determination of equivalent permeability tensors (designated k^*) for each coarse-scale grid block. Interface transmissibilities, which are required by finite-volume simulators, are then computed from the k^* in nearby grid blocks (transmissibility can be viewed as the numerical analog of permeability and involves both permeability and grid geometry). In transmissibility upscaling techniques, by contrast, the coarse-scale transmissibility at the interface (designated T^*) is determined directly in the upscaling procedure. Transmissibility upscaling has been shown to provide more accurate coarse-scale models than permeability upscaling for highly heterogeneous systems (e.g., [5, 27]). Our focus here will therefore be on transmissibility upscaling procedures.

Upscaling methods can also be distinguished in terms of the size of the domain used for the determination of the upscaled properties. In purely local upscaling, the upscaled transmissibility for the interface between two coarse grid blocks i and $i + 1$ is computed by solving a flow problem over the fine-scale domain corresponding to these two coarse blocks. Figure 1 illustrates this for a general quadrilateral grid, where the solid cells depict the local region. Note that the local region here includes all fine cells needed to form rectangular coarse blocks that cover the irregular coarse blocks.

In extended local (EL) upscaling, border regions are added around the two coarse blocks to reduce the impact of the assumed boundary conditions (e.g., [16, 19, 28, 29, 31]). In Fig. 1, for example, the EL region (indicated by the dashed lines) has a border region of one coarse-scale cell in each direction.

In global upscaling approaches, global fine-scale problems are solved to determine the coarse-scale parameters [6, 20, 24, 32]. Global upscaling techniques can
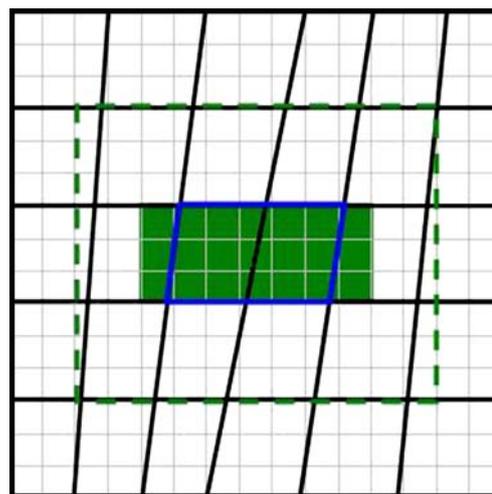

Fig. 1 A local region (*solid*) and border region (*dashed boundaries*) for a general quadrilateral coarse grid. The coarse cells are drawn in *heavier lines* and underlying fine Cartesian grid cells in *lighter lines*

provide better accuracy than local or EL procedures as they are better able to capture the effects of large-scale permeability connectivity. They do, however, require the solution of a global flow problem, which can be expensive or even prohibitive in some cases. Local–global methods comprise a family of related procedures designed to introduce global flow effects without the need for global fine-scale solutions [4, 5, 14, 30]. The use of global information in the construction of multiscale basis functions has also been shown by Efendiev et al. [11] to lead to significant improvements in multiscale finite element solutions.

Although the coarse-scale pressure equation is taken to be of the same form as the fine-scale pressure equation, significant full-tensor anisotropy can arise on the coarse scale as a result of the upscaling process, even if the fine-scale permeability is isotropic. This will occur, for example, if strong geological layering exists and this layering is skewed relative to the coarse grid. Full-tensor anisotropy can also appear from grid nonorthogonality effects. It is generally accepted that multipoint flux approximations (MPFA) are required to accurately represent full-tensor effects in finite-volume flow simulators [2, 10, 23]. These methods express the flux between two adjacent grid blocks not only in terms of the pressure in those grid blocks, as in two-point flux approximations (TPFA), but also in terms of pressures in a number of other grid blocks near the face. MPFA methods are more accurate than TPFA methods for systems with full-tensor anisotropy, but lead to increased computational costs because of wider discretization stencils. Most MPFA methods introduce a nine-point stencil in 2D and a 27-point stencil in 3D.

Standard MPFA methods do not, however, guarantee that the discretized problem results in an M-matrix, and therefore, they can lead to nonmonotonic pressure solutions [1, 25]. Such solutions are unphysical and can be problematic in practice. To address this issue, Gerritsen et al. [15] and Lambers et al. [22] proposed the variable compact multipoint approximation (VCMP). VCMP generates locally varying stencils that are optimized for flow accuracy and minimum stencil width and can be adapted to ensure certain M-matrix properties. VCMP was designed for general grid topologies, but has so far been implemented only on Cartesian and adapted Cartesian grids. In addition, it has only been used in local and EL upscaling procedures and has not been generalized for use with global upscaling. We note that ideas from VCMP have also been applied within the context of multiscale finite volume procedures [18] to improve M-matrix properties.

Our goals in this paper are to extend VCMP upscaling procedures in two important directions. Specifically, we (1) develop global VCMP techniques and (2) apply VCMP (both local and global versions) to general quadrilateral grids. Previous global transmissibility upscaling methodologies (e.g., [6, 20, 24, 32]) were presented within the context of TPFA, so they can lose accuracy when full-tensor effects are significant. Similarly, although full-tensor permeability upscaling on irregular grids has been presented [17, 28], existing techniques for transmissibility upscaling on general quadrilateral grids are based on two-point fluxes. We apply the M-fix as suggested by Gerritsen et al. [15] and Lambers et al. [22], but only when solutions are found to be nonmonotone.

All of our examples involve steady-state single-phase incompressible flow in two spatial dimensions. The simplified form of the single-phase pressure equation allows us to understand the performance and basic properties of the various schemes. The methodologies presented here are not, however, limited to single-phase flow and can be directly applied to the multiphase flow case. High accuracy for single-phase flow is a key requirement for accuracy in upscaled multiphase flow problems, so our findings are relevant for more general cases. The need for accurate upscaled transmissibilities in two-phase (oil–water) systems is well documented in previous papers (e.g., [5, 30, 32]). We also note that extension of the upscaling procedures presented here to three dimensions is straightforward. Extension of VCMP-EL methods to three dimensions is demonstrated in Lambers and Gerritsen [21].

This paper proceeds as follows. In Section 2, we present the governing pressure equation and review local and EL upscaling, TPFA discretization schemes, and the VCMP method. Then, in Section 3, we consider global upscaling and describe the use of VCMP within this context. Extensive numerical results are presented in Section 4. We consider multiple realizations of oriented Gaussian and channelized permeability fields, with flow driven by several different boundary specifications, and regular and irregular grids. The enhanced accuracy of our new procedures is clearly illustrated. Additional discussion and conclusions are presented in Sections 5 and 6.

2 Local and EL upscaling methods

2.1 Single-phase pressure equation

We consider steady-state incompressible single-phase flow in the absence of gravity and source terms. The governing dimensionless fine-scale pressure equation derives from Darcy's law ($u = -\frac{k}{\mu} \cdot \nabla p$) combined with mass conservation for an incompressible system ($\nabla \cdot u = 0$), with u being the Darcy velocity and p the pressure. The pressure equation is then given as

$$\nabla \cdot (k \cdot \nabla p) = 0. \tag{1}$$

Upscaling is required because k varies over a wide range of spatial scales. The coarse-scale pressure equation is of the same form as Eq. 1, with k replaced by k^*. Our upscaling computations involve the solution of Eq. 1 over a particular domain, and the subsequent determination of upscaled parameters (k^* or T^*) from appropriate integration of u and p.

2.2 Coarse models with TPFAs

We now discuss the use of local or EL transmissibility upscaling to provide coarse models described by TPFA. This requires the solution of Eq. 1 in a local or EL fine-scale region, as illustrated in Fig. 1. Constant-pressure boundary conditions are imposed at the inlet and outlet, and no-flow boundary conditions are prescribed on the remaining boundaries (other boundary specifications are also possible). Assuming that the flux is related only to the pressures of the two cells adjacent to the face (Fig. 2), we compute an upscaled transmissibility as

$$T^* = \frac{f^c}{p_1^c - p_2^c}, \tag{2}$$

where T^* is the TPFA upscaled transmissibility and $p_1^c = \langle p \rangle_1$ and $p_2^c = \langle p \rangle_2$ represent the area-averages of

Fig. 2 The *red dots* denote the centers of quadrilateral grid blocks that are used to construct a TPFA to the flux across a face, indicated by the *thick red line*
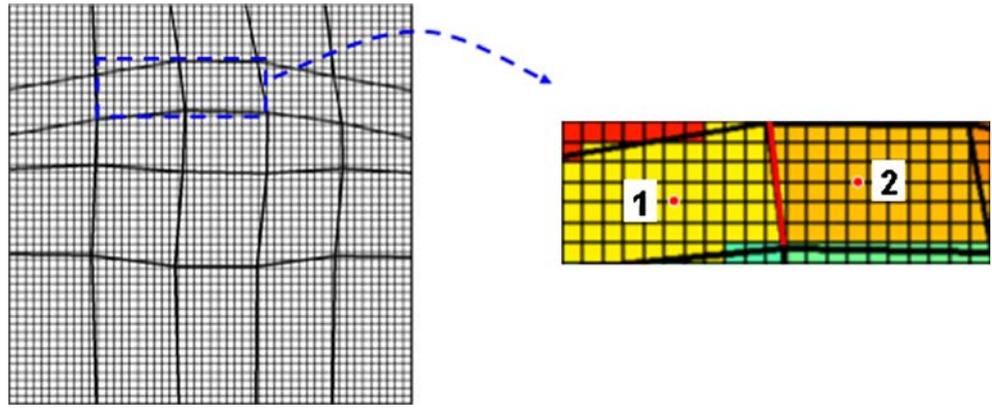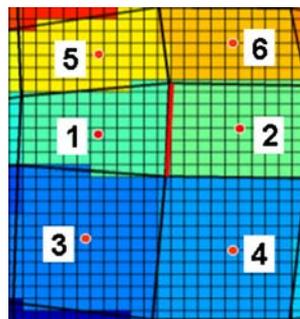

the fine-scale pressures over the regions corresponding to the two coarse cells. The flux across the region corresponding to the coarse-cell face, f^c, is obtained by integrating the fine-scale fluxes over the face; i.e., we compute $\int_l u \cdot n \, dl$, where l designates the coarse-cell face and n is the unit normal to the face. When the coarse and fine grids are not aligned, a linear interpolation of the components of u in the appropriate fine-scale cell is used to determine u along the face.

The above description is for a local flow in the x direction. A similar procedure is applied to compute the transmissibility in the y direction, using a local flow problem driven by a pressure difference in y.

2.3 Coarse models with VCMP flux methods

The TPFA may lead to large upscaling errors if there is strong anisotropy. To obtain an accurate representation of full-tensor permeability anisotropy, a transmissibility upscaling method for MPFAs was developed in Lambers et al. [22]. The stencil of this VCMP flux approximation is allowed to vary from cell to cell.

In contrast to TPFA, the transmissibility approximations include not just two but up to six averaged pressure values, as illustrated in Fig. 3. Thus,

$$f^c = -t^T p^c, \tag{3}$$

where t is the transmissibility vector, $t = [t_1, t_2, ..., t_6]^T$, and p^c contains the six averaged coarse pressure values, that is, $p^c = [p_1^c, p_2^c, ..., p_6^c]^T$ (note that we use lowercase t here to distinguish these MPFA transmissibilities from TPFA transmissibilities and that, although these t_j, $j = 1, ..., 6$ are upscaled quantities, we drop the $*$ superscript for conciseness). We use two main criteria to find the transmissibility coefficients t_j. First, they are computed to honor closely two fluxes $(f^c)_i$, $i = 1, 2$ across the coarse-cell face that result from generic flow problems on the EL region with flow driven in the x and y directions, respectively. The fluxes $(f^c)_i$, $i = 1, 2$ are found by integrating the computed fine-scale fluxes over the coarse-cell face. Second, the transmissibility coefficients t_j are required to lead, when possible, to a TPFA. Additional and necessary constraints on the t_j and their signs are imposed for consistency. Thus, we find a solution by solving the optimization problem

$$\min_t \sum_{i=1}^2 \alpha_i^2 \left| (t^T p^c)_i + (f^c)_i \right|^2 + \sum_{j=3}^6 \beta_j^2 t_j^2, \tag{4}$$

under the linear constraints

$$\sum_{j=1}^6 t_j = 0, \qquad t_{2j-1} \leq 0, \qquad t_{2j} \geq 0, \qquad j = 1, 2, 3. \tag{5}$$

The weights α_i and β_j in VCMP-EL are free to be chosen. Here, we elect to take them as $|(f^c)_i|$ and $(|f_1^c| + |f_2^c|)/M$, respectively, where M is a tuning

Fig. 3 The *red dots* denote the centers of quadrilateral grid blocks that are used to construct a VCMP approximation to the flux across a face, indicated by the *thick red line*

parameter. Large values of M lead to transmissibility weights that better resolve the two local flows, while small values of M drive the method toward a TPFA representation. Here, we use $M = 1,000$ to emphasize accuracy. The resulting VCMP stencils vary from cell to cell in terms of the number of points included and the values of the corresponding transmissibility weights.

Equating the sum of the fluxes across all faces of each coarse cell, so as to honor Eq. 1, leads to the matrix–vector equation $Ap = b$, with p as the vector of unknown pressures and b as a vector determined by the boundary conditions. The elements of A depend on the transmissibility weights.

As discussed in Section 1, unlike TPFA, MPFA methods do not necessarily lead to a monotone pressure field. In Gerritsen et al. [15], it was therefore suggested to apply a correction to the matrix elements of A to make it an M matrix, hence guaranteeing monotonicity. Sufficient conditions for A to be an M matrix are that

$$a_{k,k} > 0, \quad \forall k, \tag{6}$$

$$a_{k,l} \leq 0, \quad \forall k, l, \quad k \neq l, \tag{7}$$

and the row sums must satisfy

$$\sum_l a_{k,l} \geq 0, \quad \forall k, \tag{8}$$

with strict inequality for at least one row. Thanks to the sign constraints imposed on the weights, the diagonal elements of A are already guaranteed to be positive, so Eq. 6 is automatically satisfied.

If we can ensure that Eq. 7 is also satisfied, then the condition in Eq. 8 is satisfied as well. The first condition in Eq. 5 implies that the row sum will be zero if row k corresponds to a cell without boundary faces, and positive for a cell with a boundary face, because, in view of the inequality constraints in Eq. 5, only negative contributions to matrix elements will be omitted due to the boundary conditions.

Therefore, we only have to fix the wrongly signed off-diagonal elements to obtain an M-matrix. Each off-diagonal element of A is composed of nonnegative and nonpositive transmissibilities and can be written as:

$$a_{kl} = \sum_{j=1}^{m_{kl}^+} t_{j,kl}^+ + \sum_{j=1}^{m_{kl}^-} t_{j,kl}^-, \tag{9}$$

where each $t_{j,kl}^+ \geq 0$ and each $t_{j,kl}^- \leq 0$. Let $\tilde{a}_{kl}$ be the (k, l) entry of the updated matrix $\tilde{A}$. To guarantee that $\tilde{A}$ is an M-matrix, we impose the constraints

$$|\tilde{t}_{j,kl}^-| \geq |t_{j,kl}^-|, \qquad |\tilde{t}_{j,kl}^+| \leq \frac{1}{m_{kl}^+} \left(\sum_{j=1}^{m_{kl}^+} |t_{j,kl}^-| \right), \tag{10}$$

in addition to Eq. 5, and then recompute t_j. This predictor–corrector step is called the M-fix.

It is important to note that we can guarantee monotonicity for all possible boundary conditions by imposing the M-fix on the matrix resulting for Dirichlet boundary conditions on the entire boundary. This is due to the fact that, for any face on which Neumann boundary conditions are imposed, potential positive contributions to off-diagonal elements are not included in Eq. 10, whereas such stencils are included in the analysis when only Dirichlet boundary conditions are imposed.

In our implementation, we do not indiscriminately apply the M-fix. The above M-fix constraints, which are sufficient but not always necessary to guarantee monotonicity, can affect upscaling accuracy in some cases. Therefore, we choose to only apply the M-fix when the computed discrete solutions are indeed non-monotone, that is, when there is at least one discrete pressure value $p_{i,j}$ that is a local maximum or minimum when compared to its direct neighbors $p_{i\pm1,j\pm1}$. We refer to this as the selective M-fix.

2.4 Algorithms for VCMP-local and VCMP-EL

The algorithms for VCMP combined with local and EL upscaling are given as follows:

1. For each face of the coarse grid, define a fine-scale local or EL region. The local region for VCMP methods is the smallest rectangle containing the six coarse cells surrounding the face, shown in Fig. 3. For VCMP-EL, we add one coarse-scale cell along the dimension that is approximately perpendicular to the face.
2. Solve two local fine-scale flows Eq. 1 with two sets of generic boundary conditions on the local regions: constant pressure in one coordinate direction and no-flow in the other coordinate direction.
3. Find the six coarse-scale pressure values, p^c, and coarse-scale fluxes on the face, f^c, from these local fine-scale solutions through averaging and integration, respectively.
4. Solve the optimization problem Eq. 4 with the constraints in Eq. 5 to compute VCMP transmissibility vectors, $t = [t_1, t_2, ..., t_6]^T$. In the rare case that the

optimization problem cannot be solved, we simply use two-point flux solutions, described in Eq. 2, as substitutes.

5. Once transmissibilities are determined for each coarse-grid face, solve the coarse-scale pressure equation. Check if the pressure solution is monotone and apply the M-fix if necessary.

3 Global and iterative global upscaling methods

Global upscaling approaches use a fine-scale global solution to determine transmissibilities for coarse-scale faces. They generally provide better upscaling accuracy than (extended) local methods because connectivities at scales larger than the (extended) local regions are now included in the transmissibility calculations. The price to pay for this increased accuracy is the global solution on the geocellular grid. As compared to the full multiphase reservoir simulation, however, the computational costs associated with this solution may be acceptable.

In direct global upscaling with the TPFA, which we refer to as TPFA-DG, a fine-scale flow problem is solved over a global region. The imposed boundary conditions may be either generic (e.g., $p = 1$ at the left boundary, $p = 0$ at the right boundary, no-flow elsewhere) or they may mimic those to be used in the eventual multiphase flow simulations. Following the flow solution, the coarse-scale transmissibilities are calculated directly from Eq. 2. This approach does not guarantee that all T^* will be positive, and in the general case, some number of negative T^* will occur. When a $T^* < 0$ is observed, we replace it with T^* computed using the TPFA-EL method. This replacement of negative transmissibilities, however, acts to reduce upscaling accuracy. If there are very few (or zero) negative T^*, TPFA-DG tends to give highly accurate approximations to the averaged fine-scale solutions.

Other strategies also exist for eliminating negative transmissibilities, and these can provide better accuracy than the use of TPFA-EL. One such approach, referred to as TPFA-iterative global (TPFA-IG), iteratively adjusts the T^* from TPFA-DG using global coarse-scale solutions [6]. The goal of TPFA-IG is to match the fluxes from the global fine-scale reference solution. Designating the integrated global fine-scale flux for a particular coarse-scale interface as f_G, TPFA-IG computes the upscaled transmissibility for this interface at the next iteration as

$$\left(T^*\right)^{\nu+1} = \frac{f_G}{\left(p_1^c\right)^\nu - \left(p_2^c\right)^\nu}, \tag{11}$$

where $\left(p_1^c\right)^\nu$ and $\left(p_2^c\right)^\nu$ represent the coarse-block pressures in the two cells sharing the target interface at the previous iteration (ν). TPFA-IG can provide highly accurate flux approximations, but some accuracy in the coarse-scale pressure is generally lost in the iterative process, as the goal of the procedure is to match fluxes, not pressures.

As indicated earlier, previous global transmissibility upscaling procedures rely on TPFA approximations. Our goal here is to incorporate MPFA (specifically, VCMP) into global upscaling. This should lead to better accuracy, particularly in cases with strong full-tensor effects. Here, we propose two new algorithms that generalize their TPFA counterparts: VCMP-direct global (VCMP-DG) and VCMP-iterative global (VCMP-IG). Although the methods vary in terms of computational cost, coding effort, and accuracy, both are suitable for upscaling of heterogeneous permeability fields with full-tensor anisotropy.

As discussed in Section 2.3, VCMP requires two flow solutions. In our first implementation of VCMP with global flow information, we used two fine-scale global flows with generic boundary conditions: one with a linear pressure drop in the x direction and one with a pressure drop in the y direction. However, we observed that, in some cases, these two global flows did not provide sufficiently dissimilar local flows. This is especially true in strongly channelized systems. Also, the transmissibilities computed in this way did not lead to high accuracy for flow problems driven by other global boundary conditions. In our current implementation, we first perform a single global fine-scale flow simulation (the boundary conditions used for this solution could correspond to those to be used for the eventual multiphase flow simulations). For each coarse face, we then choose a complementary local fine-scale flow. This local flow is driven by a pressure gradient that is approximately orthogonal to the pressure gradient imposed by the global flow. The two flows thus provide complementary information that is used to construct the VCMP stencil. The VCMP-DG and VCMP-IG algorithms are outlined below.

3.1 Algorithm for VCMP-DG

Combining direct global upscaling with VCMP leads to the following algorithm:

1. Solve a global fine-scale flow problem with specified boundary conditions. Determine coarse-scale pressure, p_G, and flux, f_G.
2. For each face of a coarse-scale grid, calculate the averaged pressure gradients, $[\partial p_G/\partial x, \partial p_G/\partial y]$,

across the extended region. Select a complementary local fine-scale flow with pressure gradients $[\partial p_L/\partial x, \partial p_L/\partial y] = [-\partial p_G/\partial y, \partial p_G/\partial x]$, and solve it. Determine coarse-scale p_L and f_L.

3. Solve the optimization problem Eq. 4 honoring the two flows (p_G and f_G, p_L and f_L), with the constraints in Eq. 5, to find the VCMP transmissibility, $t = [t_1, t_2, ..., t_6]^T$. In the rare case that the optimization problem cannot be solved, we use the transmissibility from a VCMP-EL method as a substitute.

4. Check if the pressure solution is monotone. If not, find the wrongly signed elements in A and recompute the transmissibilities across the contributing faces using the additional M-fix constraints in Eq. 10.

3.2 Algorithm for VCMP-IG

In VCMP-IG, we combine VCMP with the iterative global upscaling method introduced in [6]. We iteratively adjust the transmissibility coefficients resulting from a VCMP-DG step to improve the match between the fluxes from the coarse scale solution and the global fine-scale reference solution. The approach is analogous to TPFA-IG Eq. 11. As in TPFA-IG, we expect that VCMP-IG leads to improved flux approximations. However, during the iterative adjustment of the fluxes, the accuracy in the pressure solution may reduce, as is often the case in TPFA-IG.

The complete VCMP-IG algorithm is given by

1. Solve a global fine-scale flow problem with specified boundary conditions. Compute the coarse-scale pressure, p_G^0, and flux, f_G, to be used in the transmissibility calculations. Here, f_G is the global reference solution that VCMP-IG pursues by adjusting coarse-scale transmissibilities.
   Set the iteration number $\nu = 0$.

2. For each face of a coarse-scale grid, solve a local fine-scale flow complementary to the global flow, as described in step 2 of the VCMP-DG algorithm. The solution of this local flow is denoted as p_L^ν and f_L^ν.

3. Solve the optimization problem Eq. 4 honoring the two flows (p_G^ν and f_G, p_L^ν and f_L^ν), with the constraints in Eq. 5, to find the VCMP transmissibility, $t^{\nu+1} = [t_1^{\nu+1}, t_2^{\nu+1}, ..., t_6^{\nu+1}]^T$. When the optimization problem cannot be solved, $t^{\nu+1}$ is replaced by the transmissibility from the last iteration t^ν. For the initial step $\nu = 0$, t^0 is calculated from a VCMP-EL method.

4. Check if the pressure solution is monotone. If not, find the wrongly signed elements in A and obtain the recomputed transmissibilities, $t^{\nu+1}$, across the contributing faces using the additional M-fix constraints in Eq. 10.

5. Using $t^{\nu+1}$, solve global coarse-scale flow problems, with the same specified boundary conditions as used in step 1, to obtain a coarse-scale pressure solution, and assign it to $p_G^{\nu+1}$.

6. If not converged, set $\nu = \nu + 1$ and iterate through steps 2–5.

The convergence criteria are based on the difference between the VCMP-IG solution and the reference fine-scale solution or the change in the VCMP-IG solution between iterations. For the results shown in Section 4, the following criterion is used. We stop the iteration if

$$\max\left(\frac{\parallel p_G^\nu - p_G^{\nu-1} \parallel_2}{\parallel p_G^\nu \parallel_2}, \frac{\mid Q^\nu - Q^{\nu-1} \mid}{\mid Q^\nu \mid}\right) \leq 0.01, \quad (12)$$

where ν is an iteration counter, Q is the total flow rate at the boundary from the coarse-scale model, and p_G is coarse-scale pressure. In most cases, it takes three to five iterations to converge. Fast error reduction is achieved in the initial two iterations. Since iterative global upscaling methods are designed to enhance accuracy in fluxes (while usually resulting in accuracy reduction in pressures), different convergence criteria can be chosen depending on the choice of error tolerance for fluxes and pressures.

VCMP global upscaling methods are similar to VCMP-EL except for the flow problems to be honored. VCMP global methods use one global flow and one complementary local flow, while VCMP-EL uses two generic local flows. The parameter α, introduced in Eq. 4, is defined differently for the local vs global methods. For VCMP-EL, the two local flows are weighted based on their flow rates. In VCMP-DG and VCMP-IG, $\alpha_G = n \times \mid f_L/f_G \mid$ and $\alpha_L = 1$ such that the global flow is honored more than the local flow. Here, n is a number between one (weighting the global and local flows equally in the optimization procedure) and infinity (only using the global flow), which can be tuned for different geologies. Large values of n give high accuracy for the global flow used to compute upscaled transmissibility, while small values of n provide more robustness in the upscaled model as the resulting VCMP transmissibility takes into account the two dissimilar flows equally in the optimization procedure. Results are not highly sensitive to n, though this parameter can have an impact on accuracy. In the results below,

for log-normally distributed permeability fields, we use $n = 5$, and for channelized models, we use $n = 20$. Even though this weights the global flow much more than the local complementary flow, the resulting solutions from VCMP global methods were found to be more robust than TPFA global methods due to the extra information provided by the local flow and the flexible multipoint character of VCMP.

4 Numerical results

We now test the performance of the existing and newly proposed local and global upscaling methods on a range of examples on both Cartesian and irregular structured grids.

4.1 Test suite

Our test suite consists of two types of fine-scale permeability fields:

– Twenty-five realizations of log-normally distributed permeability fields, generated by sequential Gaussian simulation [8]. All log-normal cases have dimension 100×100 on a unit square. The dimensionless correlation lengths are $\lambda_1 = 0.5$ and $\lambda_2 = 0.02$. The variance of $\log k$ is 3.0 and the mean is also 3.0. The direction of the long correlation is misaligned with the grid with an angle θ, relative to the x axis. This misalignment results in permeability anisotropy in the coarse-scale model, meaning that full-tensor effects are expected to be important when θ differs appreciably from zero. Here, we use $\theta = 30°$. Figure 4a shows a typical realization. All realizations are upscaled to 10×10 coarse grids that are either Cartesian or general quadrilateral grids. We additionally investigated the process dependency of the various upscaling methods.
– Fifty channelized layers from the SPE 10 Comparative Solution Project [7]. The permeability field of a typical channelized layer is presented in Fig. 4b. The fine grids are of dimension 220×60, with $\Delta x = 10$ and $\Delta y = 20$. The models are upscaled to 22×6 coarse grids that are either Cartesian or general quadrilateral grids.

On these fields, we apply all VCMP type methods (VCMP-EL, VCMP-DG, and VCMP-IG) and their TPFA analogs (TPFA-EL, TPFA-DG, and TPFA-IG). The size of the border regions used in TPFA-EL is as shown in Fig. 1. The border regions for VCMP-EL are the same so the results are directly comparable.
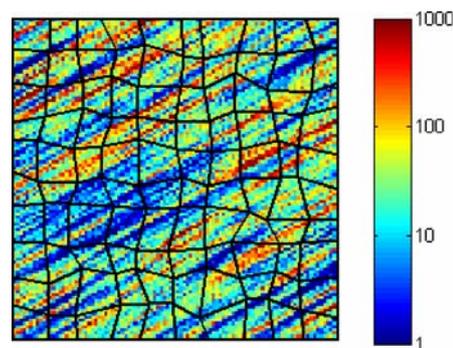
(a) Log normal permeability
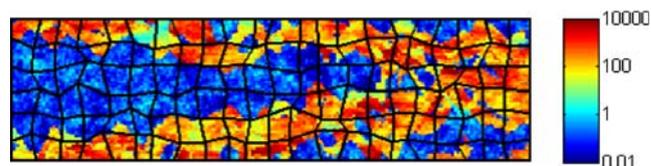
(b) Channelized permeability

Fig. 4 Fine-scale permeability fields and random grids for **a** log-normally distributed permeability realization with correlation lengths $\lambda_1 = 0.5$ and $\lambda_2 = 0.02$ and a layering orientation angle $\theta = 30°$ and **b** channelized layer (layer 44 from SPE 10)

We consider both uniform Cartesian grids and irregular grids. Starting with a uniform grid with node spacings Δx_c and Δy_c, the coarse irregular grids are generated by perturbing each node in the x direction by $\xi \Delta x_c$ and in the y direction by $\xi \Delta y_c$, where ξ is a random number within $[-0.3, 0.3]$. The boundary nodes are limited to move in only one direction. Examples of these grids are illustrated in Fig. 4. When these grids are applied, a different random grid is generated for each permeability realization.

For each permeability field and each grid, we solve the pressure equation with four sets of boundary conditions:

– Constant pressure/no-flow boundary conditions in the x and y directions, respectively. For the x direction flow, we set $p(0, y) = 1$, $p(L_x, y) = 0$, and $u_y(x, 0) = u_y(x, L_y) = 0$. For the y direction flow, we set $p(x, 0) = 1$, $p(x, L_y) = 0$, and $u_x(0, y) = u_x(L_x, y) = 0$. Here, L_x and L_y designate system lengths.
– Corner-to-corner flows. For example, for flow from the lower-left corner to the upper-right corner of a log-normal permeability field, we prescribe $p = 1$ for $0 \le y/L_y \le 0.2$, $x = 0$ and $0 \le x/L_x \le 0.2$, $y = 0$; $p = 0$ for $0.8 \le y/L_y \le 1$, $x = L_x$ and $0.8 \le x/L_x \le 1$, $y = L_y$; and no-flow conditions elsewhere. This boundary condition is also called "along layering" flow because it is aligned

Table 1 Relative errors for total flow rate, E_Q, using various upscaling methods for 25 realizations of log-normal permeability fields, on 10×10 Cartesian grids

Flow	TPFA-EL	VCMP-EL	TPFA-DG	VCMP-DG	TPFA-IG	VCMP-IG
In x direction	0.103	0.047	0.057	0.00003	0.0006	0.00003
In y direction	0.084	0.016	0.030	0.0002	0.0003	0.0002
Along layering	0.434	0.139	0.044	0.002	0.0001	0.001
Across layering	0.241	0.060	0.019	0.0001	0.0001	0.0001

with the layer orientation of the log-normally distributed permeability fields. The boundary conditions for flow from the upper-left corner to the lower-right corner are defined similarly. This is called "across layering" flow. For channelized layers, we define "along layering" and "across layering" flows similarly, except that we fix pressure over two coarse-scale cells instead of the x and y ranges given above.

A variant on lower-left to upper-right flow is introduced to assess process dependency. For this case, we prescribe $p = 1$ for $0 \leq y/L_y \leq 0.5$, $x = 0$; $p = 0$ for $0.5 \leq y/L_y \leq 1$, $x = L_x$; and no-flow conditions elsewhere. This scenario is referred to as "corner flow" and is used on log-normal permeability models.

Unless otherwise stated, in the tables below, we report the average relative errors for total flow rate through the system (E_Q) and L_2 flux and pressure errors (E_f and E_p) for the upscaled models averaged over all realizations. All errors are computed relative to the reference fine-scale solutions. The errors are defined as:

$$E_Q = \frac{|Q - Q_{\text{ref}}|}{|Q_{\text{ref}}|}, \qquad E_f = \frac{\|f - f_{\text{ref}}\|_2}{\|f_{\text{ref}}\|_2},$$
$$E_p = \frac{\|p - p_{\text{ref}}\|_2}{\|p_{\text{ref}}\|_2}, \tag{13}$$

where Q, f, and p designate the coarse-scale solutions and Q_{ref}, f_{ref}, and p_{ref} are analogous quantities computed from the fine-scale solutions. Specifically, f_{ref} is obtained by integrating fine-scale fluxes along the face of each coarse cell and p_{ref} is computed as the area-weighted average of the fine-scale pressures corresponding to each coarse cell.

All results shown below are computed with the selective M-fix, unless otherwise stated. A comparison of the original M-fix with the selective M-fix is shown in Section 4.2.3.

4.2 Log-normal permeability fields

We now present detailed upscaling results for log-normal permeability fields on Cartesian and irregular grids. VCMP-EL has already been demonstrated to be a promising approach for upscaling on Cartesian grids by Lambers et al. [22]. Here, we include the results of VCMP-EL and TPFA-EL for completeness, though our emphasis is on the new upscaling strategies, VCMP-DG and VCMP-IG, and their performance relative to TPFA-DG and TPFA-IG.

4.2.1 Results for cartesian grids

Tables 1, 2, and 3 display the mean errors in the total flow rate, flux, and pressure, respectively, using various upscaling methods for 25 realizations of the log-normal permeability fields with $\theta = 30°$. Results are reported for four sets of boundary conditions. We note first that TPFA-EL displays large errors, particularly for flow rate and flux, and these are reduced significantly through the use of VCMP-EL. This is consistent with the results reported by Lambers et al. [22]. Note that the VCMP results in Lambers et al. [22] may have unphysical oscillations because the monotonicity fix was not applied, while all results presented in this paper are oscillation-free thanks to the use of the full M-fix or selective M-fix.

Next, we compare VCMP global upscaling methods to their TPFA counterparts. We observe that VCMP-DG provides improvement over TPFA-DG for all

Table 2 L_2 flux errors, E_f, using various upscaling methods for 25 realizations of log-normal permeability fields, on 10×10 Cartesian grids

Flow	TPFA-EL	VCMP-EL	TPFA-DG	VCMP-DG	TPFA-IG	VCMP-IG
In x-direction	0.433	0.064	0.379	0.0003	0.026	0.0003
In y-direction	0.437	0.106	0.377	0.0009	0.026	0.0008
Along layering	0.519	0.236	0.204	0.010	0.007	0.005
Across layering	0.369	0.186	0.213	0.0004	0.016	0.0004

Table 3 L_2 pressure errors, E_p, using various upscaling methods for 25 realizations of log-normal permeability fields, on 10×10 Cartesian grids

Flow	TPFA-EL	VCMP-EL	TPFA-DG	VCMP-DG	TPFA-IG	VCMP-IG
In x-direction	0.133	0.012	0.120	0.00004	0.165	0.0001
In y-direction	0.121	0.013	0.098	0.0001	0.130	0.0003
Along layering	0.113	0.074	0.063	0.004	0.074	0.012
Across layering	0.069	0.035	0.027	0.0001	0.038	0.0002

quantities considered. In particular, VCMP-DG gives much more accurate results for flux and pressure than TPFA-DG, as indicated by the very small E_f (Table 2) and E_p (Table 3) values for all four boundary conditions.

TPFA-IG gives low errors for total flow rate and flux, though the flow rate and flux errors using VCMP-IG are generally even smaller. The pressure errors using TPFA-IG are larger than the pressure errors using TPFA-DG. This is as expected because, during the iterations, flux errors are minimized at the expense of pressure errors. Pressure errors using TPFA-IG are significant for x-direction and y-direction flows (E_p=0.165 and 0.130, respectively). These errors essentially vanish after applying VCMP-IG.

Because of the strong anisotropy in the coarse-scale models, which results from the oriented layering in the fine-scale permeability fields, accurate full-tensor upscaling is important for this case. For this reason, VCMP methods consistently outperform their TPFA analogs.

Among the VCMP-type methods, VCMP-EL shows the largest errors in total flow rate, local flux, and local pressure. VCMP-DG and VCMP-IG both improve upon VCMP-EL because they incorporate global flow information in the upscaling process. VCMP-IG re-

duces the L_2 flux errors associated with VCMP-DG but leads to larger errors in pressure, as expected. Overall, both VCMP-DG and VCMP-IG give small errors in both flux and pressure ($E_f \leq 0.010$ and $E_p \leq 0.012$).

The L_2 flux errors presented in the tables above represent averages of all of the flux errors in a particular model (and the subsequent average over all 25 realizations). We now present face-by-face comparisons of flux for particular models. In Fig. 5, we plot coarse-scale fluxes vs integrated fine-scale fluxes for x-direction flows for two layers. We compare results using TPFA-DG (represented by plus signs) and VCMP-DG (represented by circles). Figure 5a is for the layer with the largest L_2 flux error using TPFA-DG and Fig. 5b is for the layer with L_2 flux error nearest the average value reported in Table 2. The improvement resulting from VCMP-DG, and the high level of accuracy of the VCMP-DG results, are clearly evident in both cases.

We next illustrate the performance of TPFA-IG and VCMP-IG through visualization of the coarse-scale pressure solutions. Again, we consider worst-case (Fig. 6) and typical (Fig. 7) scenarios. The fine-scale results are averaged onto the coarse grid for easier comparison. Significant improvement using VCMP-IG is clearly evident in Fig. 6, where it is apparent that TPFA-IG is not able to accurately capture the effects of

Fig. 5 Comparison of integrated fine-scale flux and coarse-scale flux (x-direction flow, Cartesian grids) (**a**, **b**)
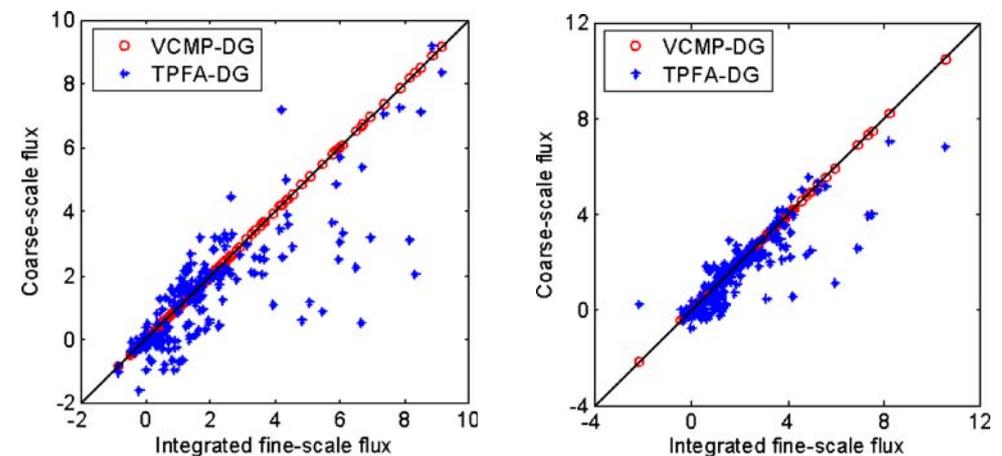
(a) Realization with the largest flux error using TPFA-DG

(b) A typical realization

Fig. 6 Pressure fields for the realization with the largest pressure error using TPFA-IG (*x*-direction flow, Cartesian grids) (**a–c**)

(a) Averaged fine-scale pressure

(b) Coarse pressure from TPFA-IG

(c) Coarse pressure from VCMP-IG
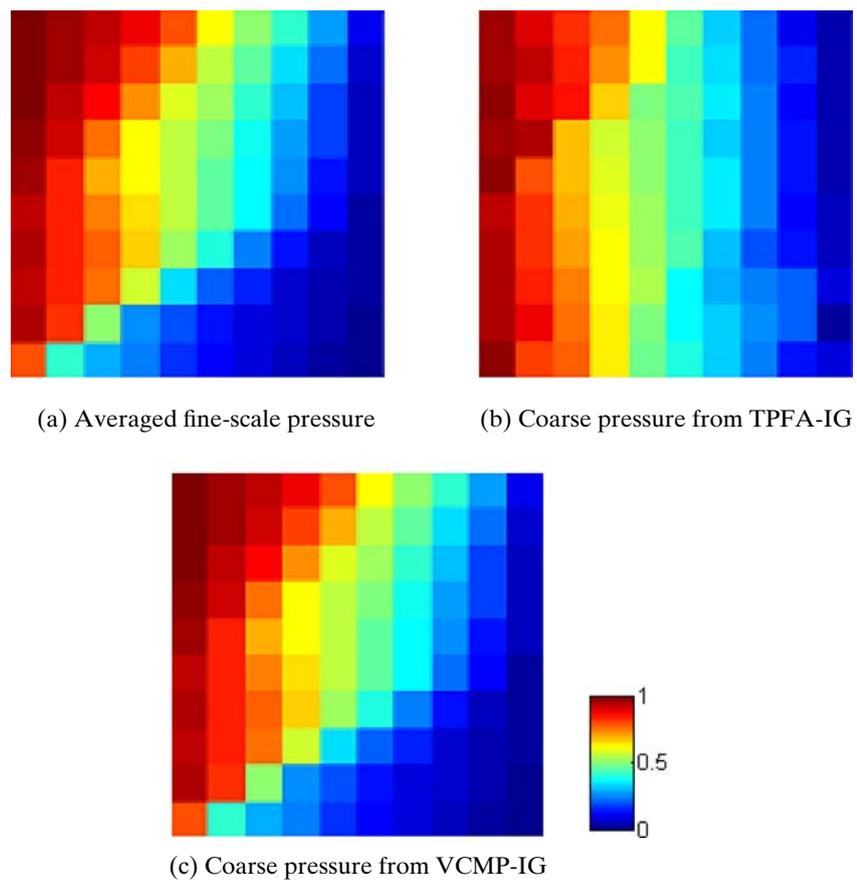
anisotropy. Improvement can also be observed in Fig. 7, where TPFA-IG again appears limited in representing oriented pressure contours. These results, along with those in Fig. 5, demonstrate that the global VCMP methods are indeed well suited for the accurate modeling of coarse systems with strong full-tensor effects.

TPFA-DG and TPFA-IG were designed for use with global flows identical or very similar to the flow used to generate the upscaled model. In Gerritsen et al. [15] and Lambers et al. [22], VCMP-EL was shown to perform robustly also for flows different from the generic flows used in the upscaling procedure. Here, we assess the level of robustness of the various methods, which is useful as the methods may be applied within workflows where it is difficult to update the upscaled model as flow rates or well conditions change. We generate the upscaled model using global *x*-direction flow. Results are presented for VCMP-DG, TPFA-DG, TPFA-IG, and VCMP-EL methods (for VCMP-EL, the usual generic local flows are used in the upscaling) for three additional flows.
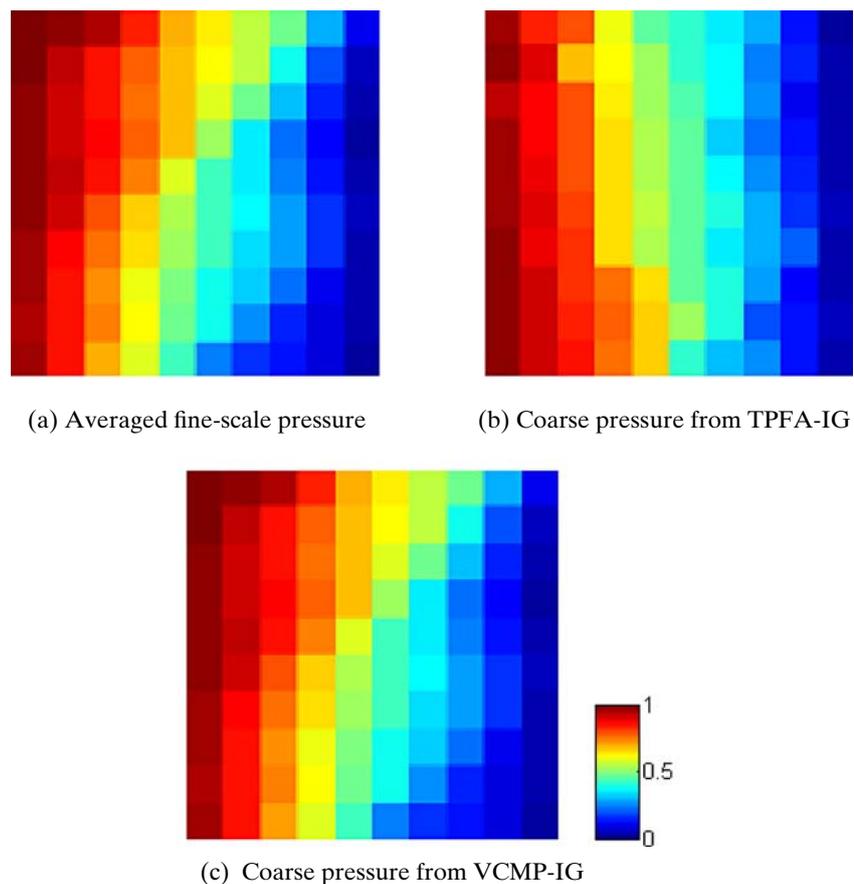
Results for flux and pressure errors are presented in Tables 4 and 5. Except for TPFA-IG for the case of *x*-direction flow (which was used to generate the

TPFA T^*), the TPFA methods generally result in significant flux errors. VCMP-DG provides results that are consistently more accurate than TPFA-IG and TPFA-DG (except for TPFA-IG flux for *x*-direction flow) and gives results that are generally comparable to VCMP-EL. This suggests that, unlike the TPFA methods, the robustness of VCMP-DG is comparable to that of VCMP-EL, which is one of the best EL methods. Similar observations hold for the pressure errors, though here, the errors using TPFA methods are not as large as they are for flux. The enhanced robustness of VCMP-DG relative to the TPFA methods is likely due in part to the fact that we use a complementary local flow problem in the determination of the upscaled transmissibilities in VCMP, which enables the upscaled model to capture effects that do not appear in the global flow, but also to its flexible multipoint character.

4.2.2 Results for irregular grids

We now demonstrate the performance of the various upscaling techniques on irregular grids. As described above, these grids are generated by randomly perturbing the nodes on uniform grids. Errors for flux and

Fig. 7 Pressure fields for a typical realization (*x*-direction flow, Cartesian grids) (**a**–**c**)

(a) Averaged fine-scale pressure

(b) Coarse pressure from TPFA-IG

(c) Coarse pressure from VCMP-IG

pressure are presented in Tables 6 and 7. Note that VCMP-EL has not been applied previously to irregular grids, so these results are also of interest.

The results for the irregular grids are very comparable to those for uniform grids (compare Tables 2 and 3). VCMP-EL consistently provides better accuracy for flux and pressure than TPFA-EL. For the global methods, TPFA-DG does not provide high accuracy for flux, though errors are quite small using the other three global methods. For pressure, the error using TPFA-IG is significant for *x*- and *y*-direction flows. This error is essentially eliminated using the global VCMP methods. Thus, in accordance with the uniform grid results, we see that the global TPFA methods are unable to consistently provide high degrees of accuracy for both flux and pressure for these anisotropic systems.

Global VCMP methods, by contrast, are designed to capture full-tensor effects and are therefore able to provide high accuracy for both flux and pressure.

4.2.3 Accuracy using M-fix and selective M-fix

As discussed in Section 2.3, the full M-fix procedure is a sufficient but not necessary condition to give a monotone pressure solution. In the results presented in this paper, we use a selective M-fix, that is, we apply the M-fix only when a nonmonotone pressure solution is found. We show here that, in some cases, the full M-fix can affect solution accuracy. Table 8 compares flow results for VCMP-EL and VCMP-DG upscaling with M-fix and selective M-fix techniques for log-normal permeability fields. The total flow rate, L_2 flux, and L_2

Table 4 Robustness test: upscaled transmissibility from flow in the *x* direction

Corner	VCMP-EL	TPFA-DG	TPFA-IG	VCMP-DG
In *x*-direction	0.072	0.379	0.026	0.033
In *y*-direction	0.135	0.716	1.965	0.294
Corner flow	0.112	0.407	0.279	0.097
Along layering	0.236	0.473	0.817	0.242

L_2 flux errors, E_f, using various upscaling methods for 25 realizations of log-normal permeability fields, on 10×10 Cartesian grids

Table 5 Robustness test: upscaled transmissibility from flow in the x direction

Corner	VCMP-EL	TPFA-DG	TPFA-IG	VCMP-DG
In x-direction	0.014	0.120	0.165	0.009
In y-direction	0.021	0.169	0.254	0.046
Corner flow	0.070	0.144	0.153	0.041
Along layering	0.076	0.221	0.349	0.097

L_2 pressure errors, E_p, using various upscaling methods for 25 realizations of log-normal permeability fields, on 10×10 Cartesian grids

pressure errors are averaged over 25 realizations. These results are for flow in the y direction. It is evident that reductions in all three errors are achieved when the selective M-fix (designated "smfix" in the table) is used in place of the full M-fix (designated "mfix"). This is the case for both the VCMP-EL and VCMP-DG methods, though the improvement is more dramatic for the DG case (for which all three errors are less than 0.1%). We reiterate that, although the A matrix generated using the selective M-fix is not an M-matrix, the pressure solution computed by solving $Ap = b$ is nonetheless, in all cases, monotonic.

The improvement offered through use of the selective M-fix is, however, not always as significant. Table 9, for example, shows y-direction flow through 50 channelized layers (considered in the next section) for which case the selective M-fix offers almost no improvement when used with VCMP-EL. Improvement with VCMP-DG, although noticeable, is fairly modest. The limited impact in this case is likely because tensor effects are not very important for these channelized models, so the results are fairly insensitive to the M-fix treatment.

4.3 Channelized permeability fields

We now consider the 50 channelized layers from the SPE 10 model. These correspond to the lower 50 layers of the 85 total layers contained in SPE 10. We consider both uniform and irregular grids. In all cases, we upscale the 220×60 fine models to 22×6 coarse models.

4.3.1 Results for cartesian grids

Table 10 presents the mean errors in total flow rate using various upscaling methods for the 50 layers. Tables 11 and 12 show L_2 flux and pressure errors.

Both VCMP-DG and VCMP-IG provide high degrees of accuracy for all quantities. For this case, TPFA-IG also provides results of reasonably high accuracy for all quantities including pressure (though pressure error for y-direction flow is 0.086). Pressure errors using TPFA-IG are generally smaller in this case than for the oriented layer case considered above. This is probably because this channelized system does not display strong anisotropy. Indeed, in over 70% of the domain, the maximum of t_3, t_4, t_5, and t_6 (see Eq. 3) is less than 10% of the maximum of t_1 and t_2. Thus, a good TPFA method such as TPFA-IG is able to capture both flux and pressure reasonably well in this case. Results for flux and pressure using VCMP-IG are, however, in all cases, more accurate than those using TPFA-IG. For the EL methods, VCMP-EL is generally more accurate than TPFA-EL for this system.

4.3.2 Results for irregular grids

The flux and pressure errors for the various upscaling methods for the 50 channelized layers of SPE 10 on random coarse grids are presented in Tables 13 and 14. VCMP-DG reduces the L_2 flux errors from TPFA-DG significantly, as shown in Table 13. VCMP-IG and TPFA-IG give results that are accurate and generally quite comparable. It appears that, even with irregular grids, the full-tensor effects for this case are not that significant, which enables TPFA-IG to provide accurate results. This is likely because the average orientation of the grids is still more or less flow-aligned. As clearly shown for the non aligned permeability fields in the previous subsection, the accuracy of TPFA-IG decreases when the full-tensor effects are stronger.

In contrast to the results on uniform grids, VCMP-EL with the selective M-fix provides low accuracy in

Table 6 L_2 flux errors, E_f, using various upscaling methods for 25 realizations of log-normal permeability fields, on 10×10 random grids

Flow	TPFA-EL	VCMP-EL	TPFA-DG	VCMP-DG	TPFA-IG	VCMP-IG
In x-direction	0.450	0.059	0.310	0.004	0.015	0.003
In y-direction	0.434	0.109	0.353	0.008	0.017	0.001
Along layering	0.531	0.232	0.156	0.026	0.002	0.010
Across layering	0.372	0.204	0.283	0.0007	0.019	0.0007

Table 7 L_2 pressure errors, E_p, using various upscaling methods for 25 realizations of log-normal permeability fields, on 10×10 random grids

Flow	TPFA-EL	VCMP-EL	TPFA-DG	VCMP-DG	TPFA-IG	VCMP-IG
In x-direction	0.132	0.013	0.098	0.0007	0.131	0.003
In y-direction	0.120	0.014	0.090	0.0005	0.115	0.001
Along layering	0.116	0.077	0.052	0.009	0.062	0.020
Across layering	0.070	0.044	0.036	0.0001	0.044	0.0006

Table 8 Flow results using VCMP-EL or VCMP-DG with full M-fix or selective M-fix, for 25 realizations of log-normal permeability fields, on Cartesian grids, with flow in the y direction

Errors	VCMP-EL-mfix	VCMP-EL-smfix	VCMP-DG-mfix	VCMP-DG-smfix
E_Q	0.138	0.016	0.092	0.0002
E_f	0.289	0.106	0.203	0.0009
E_p	0.065	0.013	0.054	0.0001

Table 9 Flow results using VCMP-EL or VCMP-DG with full M-fix or selective M-fix, for 50 realizations of SPE 10 permeability fields, on Cartesian grids, with flow in the y direction

Errors	VCMP-EL-mfix	VCMP-EL-smfix	VCMP-DG-mfix	VCMP-DG-smfix
E_Q	0.123	0.122	0.020	0.008
E_f	0.348	0.343	0.127	0.068
E_p	0.090	0.089	0.042	0.022

Table 10 Relative errors for total flow rate, E_Q, using various upscaling methods for 50 channelized layers of SPE 10, on 22×6 Cartesian grids

Flow	TPFA-EL	VCMP-EL	TPFA-DG	VCMP-DG	TPFA-IG	VCMP-IG
In x-direction	0.204	0.025	0.038	0.005	0.001	0.002
In y-direction	0.158	0.122	0.045	0.008	0.004	0.001
Along layering	0.309	0.242	0.016	0.011	0.001	0.001
Across layering	0.313	0.236	0.029	0.012	0.001	0.002

Table 11 L_2 flux errors, E_f, using various upscaling methods for 50 channelized layers of SPE 10, on 22×6 Cartesian grids

Flow	TPFA-EL	VCMP-EL	TPFA-DG	VCMP-DG	TPFA-IG	VCMP-IG
In x-direction	0.368	0.090	0.190	0.021	0.024	0.009
In y-direction	0.417	0.343	0.255	0.068	0.053	0.015
Along layering	0.484	0.369	0.195	0.052	0.033	0.013
Across layering	0.472	0.375	0.196	0.035	0.019	0.009

Table 12 L_2 pressure errors, E_p, using various upscaling methods for 50 channelized layers of SPE 10, on 22×6 Cartesian grids

Flow	TPFA-EL	VCMP-EL	TPFA-DG	VCMP-DG	TPFA-IG	VCMP-IG
In x-direction	0.086	0.028	0.043	0.008	0.046	0.020
In y-direction	0.087	0.089	0.074	0.022	0.086	0.035
Along layering	0.212	0.171	0.037	0.013	0.040	0.020
Across layering	0.200	0.103	0.039	0.010	0.046	0.021

Table 13 L_2 flux errors, E_f, using various upscaling methods for 50 channelized layers of SPE 10, on 22×6 random grids

Flow	TPFA-EL	VCMP-EL	TPFA-DG	VCMP-DG	TPFA-IG	VCMP-IG
In x-direction	0.433	0.099	0.183	0.045	0.013	0.019
In y-direction	0.478	0.881	0.342	0.095	0.065	0.023
Along layering	0.551	0.387	0.238	0.100	0.029	0.031
Across layering	0.515	0.768	0.205	0.079	0.018	0.026

Table 14 L_2 pressure errors, E_p, using various upscaling methods for 50 channelized layers of SPE 10, on 22×6 random grids

Flow	TPFA-EL	VCMP-EL	TPFA-DG	VCMP-DG	TPFA-IG	VCMP-IG
In x-direction	0.078	0.027	0.030	0.012	0.036	0.034
In y-direction	0.101	0.109	0.080	0.031	0.095	0.051
Along layering	0.227	0.182	0.040	0.026	0.051	0.045
Across layering	0.207	0.107	0.034	0.023	0.042	0.047

some cases, particularly for the y-direction flow and across layering flow. The values reported in the tables are strongly impacted by two low-flow layers, which display large errors. Eliminating these two layers, VCMP-EL is seen to provide better accuracy for flux than TPFA-EL (see Table 15).

5 Discussion

We demonstrated the significant improvements offered by global VCMP methods over their TPFA counterparts. Here, we note some additional cases that were simulated, provide some general observations, and offer some suggestions for future developments.

In addition to the extensive numerical results presented in Section 4, we also simulated several other example cases. These include log-normally distributed permeability fields with the layering oriented at 45° (rather than 30° as in the examples in Section 4) and oriented-layer cases in which the fine-scale 100×100 model was coarsened to 5×20 rather than 10×10. In both instances, results comparable to those presented in Section 4 for $\theta = 30°$ with 10×10 coarse grids were obtained (Tables 1, 2, and 3). We also evaluated the level of robustness of the upscaled channelized models (on Cartesian and random grids) and achieved results qualitatively similar to those presented in our assessment of the robustness of the oriented-layer systems (Tables 4 and 5). These observations further strengthen our findings and suggest that global VCMP methods will be broadly applicable.

Our results demonstrate very clear advantages of VCMP-DG over TPFA-DG. In typical cases, the accuracy of VCMP-DG is such that iteration on the resulting transmissibilities is really not necessary; i.e., there

is often not much need to perform VCMP-IG. The same cannot be said for TPFA-DG, which often results in significant error, so TPFA-IG is generally required. When VCMP-IG is applied, the iteration procedure is designed to force agreement only in fluxes. As a result, the pressure error generally increases. The flexibility of VCMP makes it possible, however, to devise a modified VCMP-IG procedure in which the objective of the iterations is to minimize error in both pressure and flux. The resulting coarse-scale model could then potentially provide even more accurate pressures than are currently achieved.

A number of other extensions and investigations could be considered in future work. These include an assessment of the sensitivity of the coarse-scale results to the size of the border region (we note that Wen et al. [30] demonstrated high levels of accuracy with very small border regions) and the incorporation of near-well treatments into the coarse model [4]. Testing on more extreme (high aspect ratio) grids will also be of interest. It will additionally be useful to improve our selective M-fix procedure. This will likely require the development of necessary conditions on the A matrix (short of the M-matrix requirement), which guarantee solution monotonicity. Finally, we note that extension of the methods to three dimensions is relatively straightforward. VCMP-EL and the M-fix were recently extended to three dimensions on Cartesian and adapted Cartesian grids [21].

6 Conclusions

In this paper, we developed and applied new upscaling procedures that are suitable for the accurate representation of general anisotropy (full-tensor effects) in

Table 15 L_2 flux and pressure errors, using TPFA-EL and VCMP-EL for 48 of the 50 channelized layers of SPE 10, on 22×6 random grids

Flow	E_f		E_p	
	TPFA-EL	VCMP-EL	TPFA-EL	VCMP-EL
In x-direction	0.438	0.099	0.077	0.026
In y-direction	0.476	0.295	0.101	0.106
Along layering	0.545	0.377	0.231	0.182
Across layering	0.517	0.282	0.214	0.102

coarse-scale simulation models. These approaches are based on the previously developed VCMP flux approximation technique. Two important new features were introduced in this paper: the coupling of VCMP with global flow information and the extension of VCMP procedures to irregular quadrilateral grids. A selective M-fix procedure, which enforces the M-matrix property in the upscaled coefficient matrix only when it is necessary to achieve monotone pressure solutions, was also introduced. Our specific conclusions are as follows:

– The incorporation of global flow information into VCMP procedures was shown to provide high degrees of accuracy for both pressure and flux. Two variants, the direct global (VCMP-DG) and the iterated global (VCMP-IG) methods, were introduced. For the oriented-layer fine-scale models, in which case the coarse models display significant full-tensor character, the global VCMP methods provided clear improvement relative to their TPFA counterparts (e.g., pressure errors of 4–16% reduced to 1% or less).
– The global VCMP methods use a complementary local flow in addition to a global flow in the determination of upscaled transmissibilities. As a result of this, and the flexible multipoint character of VCMP, these methods have some degree of robustness, meaning they can often provide a good level of accuracy when applied to flows with different boundary conditions. Their accuracy for such cases was shown to be comparable to that of an EL method and much better than the TPFA-IG method.
– For channelized reservoir models, TPFA-IG performed very well, and only minimal improvement was provided by global VCMP methods. This is likely because the channels are approximately oriented with the grid, and full-tensor effects are not important in this case. Thus, two-point methods can accurately approximate both pressure and flux in the coarse-scale model. Indeed, for these cases, the transmissibility weights obtained by VCMP were close to TPFA stencils for over 70% of the domain.
– It is desirable to use the selective M-fix, that is, to only update the coefficient matrix when non-monotone pressure solutions are observed. In some cases this improvement was slight, though in other cases (VCMP-DG for log normal permeability fields with $\theta = 30°$), the use of selective M-fix reduced the flow rate, flux, and pressure errors in the upscaled model significantly (from 5–20% to 0.1% or less).

References

1. Aavatsmark, I.: An introduction to multipoint flux approximations for quadrilateral grids. Comput. Geosci. **6**(3–4), 405–432 (2002)
2. Aavatsmark, I., Barkve, T., Boe, O., Mannseth, T.: Discretization on non-orthogonal quadrilateral grids for inhomogeneous, anisotropic media. J. Comput. Phys. **127**(1), 2–14 (1996)
3. Caers, J.: Petroleum Geostatistics. Society of Petroleum Engineers, Richardson (2005)
4. Chen, Y., Durlofsky, L.J.: Adaptive local-global upscaling for general flow scenarios in heterogeneous formations. Transp. Porous Media **62**, 157–185 (2006)
5. Chen, Y., Durlofsky, L.J., Gerritsen, M.G., Wen, X.H.: A coupled local-global upscaling approach for simulating flow in highly heterogeneous formations. Adv. Water Resour. **26**, 1041–1060 (2003)
6. Chen, Y., Mallison, B.T., Durlofsky, L.J.: Nonlinear two-point flux approximation for modeling full-tensor effects in subsurface flow simulations. Comput. Geosci. **12**(3), 317–335 (2008)
7. Christie, M.A., Blunt, M.J.: Tenth SPE comparative solution project: a comparison of upscaling techniques. SPE Reserv. Evalu. Eng. **4**(4), 308–317 (2001)
8. Deutsch, C.V., Journel, A.G.: GSLIB: Geostatistical Software Library and User's Guide, 2nd edn. Oxford University Press, New York (1998)
9. Durlofsky, L.J.: Upscaling and gridding of fine scale geological models for flow simulation. In: Proceedings of the 8th International Forum on Reservoir Simulation, Iles Borromees, Stresa, 20–24 June 2005
10. Edwards, M.G., Rogers, C.F.: Finite volume discretization with imposed flux continuity for the general tensor pressure equation. Comput. Geosci. **2**(4), 259–290 (1998)
11. Efendiev, Y., Ginting, V., Hou, T., Ewing, R.: Accurate multiscale finite element methods for two-phase flow simulations. J. Comput. Phys. **220**, 155–174 (2006)
12. Farmer, C.L.: Upscaling: a review. Int. J. Numer. Methods Fluids **40**, 63–78 (2002)
13. Gerritsen, M.G., Durlofsky, L.J.: Modeling fluid flow in oil reservoirs. Annu. Rev. Fluid Mech. **37**, 211–238 (2005)
14. Gerritsen, M.G., Lambers, J.V.: Integration of local-global upscaling and grid adaptivity for simulation of subsurface flow in heterogeneous formations. Comput. Geosci. **12**(2), 193–208 (2008)
15. Gerritsen, M.G., Lambers, J.V., Mallison, B.T.: A variable and compact MPFA for transmissibility upscaling with guaranteed monotonicity. In: Proceedings of the 10th European Conference on the Mathematics of Oil Recovery, Amsterdam, 4–7 September 2006
16. Gomez-Hernandez, J.J., Journel, A.G.: Stochastic charaterization of gridblock permeability. SPE Form. Eval. **9**(2), 93–99 (1994)
17. He, C., Edwards, M.G., Durlofsky, L.J.: Numerical calculation of equivalent cell permeability tensors for general quadrilateral control volumes. Comput. Geosci. **6**(1), 29–47 (2002)

18. Hesse, M., Mallison, B.T., Tchelepi, H.A.: Compact multiscale finite volume method for anisotropic heterogeneous elliptic equations. SIAM Multiscale Model. Simul. (2009, in press)
19. Holden, L., Lia, O.: A tensor estimator for the homogenization of absolute permeability. Transp. Porous Media **8**, 37–46 (1992)
20. Holden, L., Nielsen, B.F.: Global upscaling of permeability in heterogeneous reservoirs: the output least squares (OLS) method. Transp. Porous Media **40**, 115–143 (2000)
21. Lambers, J.V., Gerritsen, M.G.: Spatially-varying compact multi-point flux approximations for 3-D adapted grids with guaranteed monotonicity. In: Proceedings of the 11th European Conference on the Mathematics of Oil Recovery, Bergen, 8–11 September 2008
22. Lambers, J.V., Gerritsen, M.G., Mallison, B.T.: Accurate local upscaling with variable compact multipoint transmissibility calculations. Comput. Geosci. **12**(3), 399–416 (2008)
23. Lee, S.H., Tchelepi, H.A., Jenny, P., DeChant, L.J.: Implementation of a flux-continuous finite-difference method for stratigraphic, hexahedron grids. SPE J. **7**(3), 267–277 (2002)
24. Mallison, B.T., Chen, Y., Durlofsky, L.J.: Nonlinear two-point flux approximations for simulating subsurface flows with full-tensor anisotropy. In: Proceedings of the 10th European Conference on the Mathematics of Oil Recovery, Amsterdam, 4–7 September 2006
25. Nordbotten, J.M., Aavatsmark, I., Eigestad, G.T.: Monotonicity of control volume methods. Numer. Math. **106**(2), 255–288 (2007)
26. Renard, P., de Marsily, G.: Calculating equivalent permeability: a review. Adv. Water Resour. **20**, 253–278 (1997)
27. Romeu, R.K., Noetinger, B.: Calculation of internodal transmissibilities in finite difference models of flow in heterogeneous media. Water Resour. Res. **31**(4), 943–959 (1995)
28. Wen, X.H., Durlofsky, L.J., Edwards, M.G.: Upscaling of channel systems in two dimensions using flow-based grids. Transp. Porous Media **51**, 343–366 (2003)
29. Wen, X.H., Durlofsky, L.J., Edwards, M.G.: Use of border regions for improved permeability upscaling. Math. Geol. **35**(5), 521–547 (2003)
30. Wen, X.H., Chen, Y., Durlofsky, L.J.: Efficient 3D implementation of local-global upscaling for reservoir simulation. SPE J. **11**(4), 443–453 (2006)
31. Wu, X.H., Efendiev, Y.R., Hou, T.Y.: Analysis of upscaling absolute permeability. Discrete Contin. Dyn. Syst. Ser. B **2**(2), 185–204 (2002)
32. Zhang, P., Pickup, G., Christie, M.: A new practical method for upscaling in highly heterogeneous reservoir models. SPE J. **13**(1), 68–76 (2008)